RSC Advances

PAPER

View Article Online
View Journal | View Issue

Cite this: *RSC Adv.*, 2017, **7**, 31858

Behavior of interactions between hydrogen chalcogenides and an anthracene π-system elucidated by QTAIM dual functional analysis with QC calculations†‡

Satoko Hayashi,* Yuji Sugibayashi and Waro Nakanishi *

The nature of EH_2-*-π($C_{14}H_{10}$) interactions (E = O, S, Se and Te) of an anthracene system was elucidated by applying QTAIM dual functional analysis (QTAIM-DFA) after clarification of the structural features with quantum chemical (QC) calculations. π-HB (hydrogen bond) interactions were detected for E = O, S, Se and Te, whereas π-EB (chalcogen bond) interactions were observed for E = O in (EH_2)-*-π($C_{14}H_{10}$), where the bond paths connected H in EH_2 to $C_{14}H_{10}$ in π-HB, and they connected E in EH_2 to $C_{10}H_8$ in π-EB. The QTAIM-DFA parameters of (R, θ) and (θ_p, κ_p) were evaluated for the interactions *via* analysing the plots of $H_b(r_c)$ *versus* $H_b(r_c) - V_b(r_c)/2$ for the interactions at the bond critical points. Data obtained from the perturbed structures around the fully optimized structures were employed for the plots, in addition to the fully optimized structures. Data obtained from the fully optimized structures were analysed using (R, θ), which corresponded to the static nature, and those obtained from the perturbed structures were analysed using (θ_p, κ_p), which represented the dynamic nature of the interactions, where θ_p corresponds to the tangent line of the plot and κ_p is the curvature. The θ and θ_p values are less than 90° for all the interactions examined, except for the ^{i}H-*-^{11}C(π) interaction in TeH_2-*-$C_{14}H_{10}$ (C_1: IIB_{Atc}), where ^{i}H is located closer to the centre of $C_{14}H_{10}$. Therefore, the interactions examined were predicted to have vdW nature, appeared in the pure-CS (closed shell) interaction region, although ^{i}H-*-^{11}C(π) was predicted to have the pure-CS/typical-HB nature without covalency. Additionally, the π-HB interaction seems to be slightly stronger than π-EB in (OH_2)-*-π($C_{14}H_{10}$).

Received 14th April 2017
Accepted 19th May 2017

DOI: 10.1039/c7ra04224h

rsc.li/rsc-advances

Introduction

Significant attention has been paid to the interactions between hydrogen chalcogenides (EH_2: E = O, S, Se and Te) and aromatic π-systems, and some structures have been reported for benzene adducts formed through π-interactions.[1–8] The interactions in benzene π-systems are mainly characterized by the hydrogen bonds formed between EH_2 and the benzene π-system, which act as a proton donor and proton acceptor, respectively, and have been called hydrogen bonds of the π-type (π-HBs) herein.[1–8] The π-HB (hydrogen bond) interactions were also investigated for 1 : 1 and 2 : 1 adducts between EH_2 (E = O and S) and the naphthalene π-system.[9–20] Indeed, there have been many investigations on π-adducts, which are mainly based on a theoretical background; however, these investigations seem to be rather limited to structural features. The nature of the π-HB interactions has seldom been reported, especially for the anthracene π-system, π($C_{14}H_{10}$), to the best of our knowledge.

Very recently, we reported the nature of the $EH_2\cdots\pi$ interactions for benzene and naphthalene π-systems, together with their structural features.[1,2,10,11] The H atom(s) in EH_2 is (are) connected to the benzene π-system, $EH_2\cdots\pi(C_6H_6)$, *via* bond paths (BPs). Through careful examination of the BPs in the adducts, another type of interaction was also detected in $H_2E\cdots\pi(C_6H_6)$, where E in EH_2 is joined to the benzene π-system *via* a BP. Such interaction was called a chalcogen π-type (π-EB) bond. EH_2 is connected to the C atoms or BCPs (bond critical points: r_c: *)[21] on the C=C bonds of C_6H_6 by BPs. In the case of the benzene π-system, π-EBs seem more important relative to π-HBs, although the predicted importance may change depending on the calculation system.[2]

What happens if EH_2 (E = O, S, Se and Te) interacts with the anthracene π-system? The anthracene π-system contains two types of (three) benzene π-systems and one type of (two)

Department of Material Science and Chemistry, Faculty of Systems Engineering, Wakayama University, 930 Sakaedani, Wakayama, 640-8510 Japan. E-mail: hayashi3@sys.wakayama-u.ac.jp; nakanisi@sys.wakayama-u.ac.jp; Fax: +81 73 457 8353; Tel: +81 73 457 8252

† Dedicated to Professor Marian Mikołajczyk (Professor at the Centre of Molecular and Macromolecular Studies, Polish Academy of Sciences in Lodz, Poland) on the occasion of his 80th birthday.

‡ Electronic supplementary information (ESI) available: QTAIM-DFA approach, Cartesian coordinates for optimized structures of (EH_2)$\cdots$π($C_{14}H_{10}$) (E = O, S, Se and Te). See DOI: 10.1039/c7ra04224h

naphthalene π-system, in addition to the original anthracene π-system. What are the differences and similarities in the $EH_2\cdots\pi$ interactions between the anthracene π-system and the π-systems of naphthalene and benzene? The nature of the interactions in $(EH_2)\cdots\pi(C_{14}H_{10})$ (E = O, S, Se and Te) is elucidated together with its structural feature. Scheme 1 illustrates some of the structures expected for (EH_2)-*-$\pi(C_{14}H_{10})$ of the 1 : 1 adducts, which are inferred from the structures of (EH_2)-*-$\pi(C_{10}H_8)$ and (EH_2)-*-$\pi(C_6H_6)$. Type IIA_{Atc} and type IIC_{Atc} in $(EH_2)\cdots\pi(C_{14}H_{10})$ are defined for the adduct, where EH_2 locates on the central and outer benzene rings of anthracene, respectively, whereas it is above the ^{11}C–^{12}C (or ^{13}C–^{14}C) bond in type IIB_{Atc}. The structures for the 1 : 1 adduct of (EH_2)-*-$\pi(C_6H_6)$ and (EH_2)-*-$\pi(C_{10}H_8)$ are also shown in Scheme 1 for convenience of discussion. The optimized structures are called type Ia_{Bzn}, Ib_{Bzn} and type II_{Bzn} for (EH_2)-*-$\pi(C_6H_6)$ and type I_{Nap} and type II_{Nap} for (EH_2)-*-$\pi(C_{10}H_8)$.

The QTAIM (quantum theory of atoms-in-molecules) approach, introduced by Bader[22,23] enables the analysis of the nature of chemical bonds and interactions.[24–30] Interactions seem to be defined by the corresponding BPs, but we must be careful to use the correct terminology with the concept.[31] BCP is an important concept in QTAIM, which is a point along the BP at the interatomic surface, where charge density, $\rho(\boldsymbol{r})$, reaches a minimum.[32] It is denoted by $\rho_b(\boldsymbol{r}_c)$, in addition to other QTAIM functions at BCPs, such as Laplacians of $\rho(\boldsymbol{r})$ ($\nabla^2\rho_b(\boldsymbol{r}_c)$), total electron energy densities $H_b(\boldsymbol{r}_c)$, potential energy densities $V_b(\boldsymbol{r}_c)$ and kinetic energy densities $G_b(\boldsymbol{r}_c)$, together with $k_b(\boldsymbol{r}_c)$ ($= V_b(\boldsymbol{r}_c)/G_b(\boldsymbol{r}_c)$).

Recently, we proposed QTAIM dual functional analysis (QTAIM-DFA),[33–36] according to QTAIM.[22–30,37] QTAIM-DFA enables experimental chemists to analyse their own results concerning chemical bonds and interactions with their own image.[38] QTAIM-DFA provides an excellent possibility for evaluating, classifying and understanding weak to strong interactions in a unified form.[33–36] To elucidate the nature of the interactions in question with QTAIM-DFA, $H_b(\boldsymbol{r}_c)$ is plotted *versus* $H_b(\boldsymbol{r}_c) - V_b(\boldsymbol{r}_c)/2$ [$= (\hbar^2/8m)\nabla^2\rho_b(\boldsymbol{r}_c)$], where both the x and y axes are given units of energy. In our treatment, data for perturbed structures around fully optimized structures are employed for the plots, in addition to the fully optimized structures.[33–36] We propose the concept of "the dynamic nature of interactions" which originated from the data containing the perturbed structures.[33a,34–36,39]

Data from the fully optimized structures correspond to the static nature of interactions. QTAIM-DFA is applied to typical chemical bonds and interactions and rough criteria are established. The rough criteria can distinguish the chemical bonds and interactions in question from others. QTAIM-DFA and the criteria are explained in the ESI with Schemes S1 and S2, Fig. S1 and eqn (S1)–(S7).‡ The basic concept of the QTAIM approach is also surveyed.

QTAIM-DFA is applied to elucidate the dynamic and static nature of the interactions in (EH_2)-*-$\pi(C_{14}H_{10})$ (E = O, S, Se and Te). The discussion is limited to the 1 : 1 adducts of (EH_2)-*-$\pi(C_{14}H_{10})$ for simplicity. Herein, we present the results of the investigations on the nature of the interactions in question. The interactions are classified and characterized as a reference by employing the criteria.

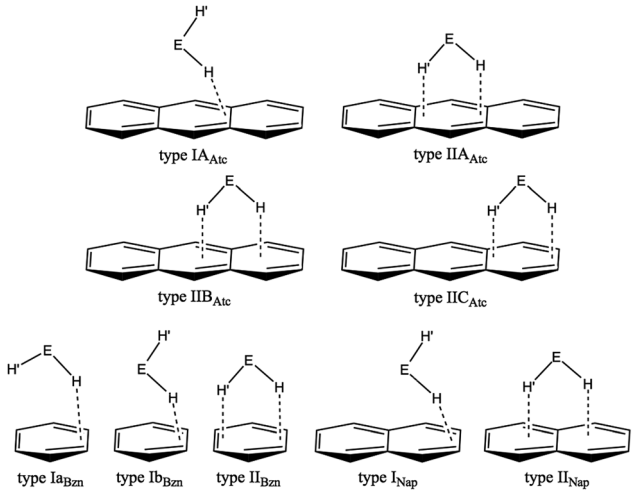

Scheme 1 Structures expected for $(EH_2)\cdots\pi(C_{14}H_{10})$ (E = O, S, Se and Te), based on that optimized for $(EH_2)\cdots\pi(C_6H_6)$ and $(EH_2)\cdots\pi(C_{10}H_8)$.

Methodological details in calculations

Structures were optimized using the Gaussian 09 programs.[40] The 6-311+G(3df) basis set[41] was employed for O, S and Se and the basis set of the (7433111/743111/7411/2 + 1s1p1d1f) type from Sapporo Basis Set Factory[42] was used for Te with the 6-311++G(d, p) basis set[41] for C and H. The basis set system (BSS) is called BSS-F according to examinations of the BSSs in a previous study. The Møller–Plesset second order energy correlation (MP2) level[43] was applied to the calculations. Optimized structures were confirmed by the frequency analysis.

QTAIM functions were calculated by employing the wfn files using the Gaussian 09 program package[40] with the same method for optimizations, and the data were analysed with the AIM2000 program.[44] The normal coordinates of internal vibrations (NIV) obtained by the frequency analysis were employed to generate the perturbed structures,[35,36] which is explained in eqn (1). The k-th perturbed structure in question ($\boldsymbol{S}_{kw}$) was generated by the addition of the normal coordinates of the k-th internal vibration ($\boldsymbol{N}_k$) to the standard orientation of a fully optimized structure ($\boldsymbol{S}_0$) in the matrix representation.[35] The coefficient f_{kw} in eqn (1) controls the difference in the structures between $\boldsymbol{S}_{kw}$ and $\boldsymbol{S}_0$: f_{kw} is determined to satisfy eqn (2) for the interaction in question, where, r and r_0 stand for the distances in question in the perturbed and fully optimized structures, respectively, with a_0 of Bohr radius (0.52918 Å). The perturbed structures with NIV correspond to that with r being elongated or shortened by $0.05a_0$ or $0.1a_0$, relative to r_0, as shown in eqn (2). $\boldsymbol{N}_k$ of five digits are used to predict $\boldsymbol{S}_{kw}$. The selected vibration must contain the motion of the interaction in question most effectively among all the zero-point internal vibrations.

$$\boldsymbol{S}_{kw} = \boldsymbol{S}_0 + f_{kw}\boldsymbol{N}_k \quad (1)$$

$$r = r_0 + wa_0\ (w = (0), \pm0.05 \text{ and } \pm0.1;\ a_0 = 0.52918\ \text{Å}) \quad (2)$$

$$y = c_o + c_1x + c_2x^2 + c_3x^3 \quad (3)$$

(R_c^2: square of correlation coefficient).

In the QTAIM-DFA treatment, $H_b(\boldsymbol{r}_c)$ is plotted *versus* $H_b(\boldsymbol{r}_c) - V_b(\boldsymbol{r}_c)/2$ for data of five points of $w = 0$, ±0.05 and ±0.1, as shown in eqn (2). Each plot is analysed using a regression curve of the cubic function, as shown in eqn (3), where $(x, y) = (H_b(\boldsymbol{r}_c) - V_b(\boldsymbol{r}_c)/2, H_b(\boldsymbol{r}_c))$ ($R_c^2 > 0.99999$ usually).[45]

Results and discussion

Structural feature of $(EH_2)\cdots\pi(C_{14}H_{10})$ (E = O, S, Se and Te)

Before the final structural optimizations for (EH_2)-*-$\pi(C_{14}H_{10})$ (E = O, S, Se and Te), the minima were searched for systematically with MP2/BSS-F. The search was started assuming typically type IIA_{Atc}, type IIB_{Atc} and type IIC_{Atc} structures of the C_1 symmetry. The type IIA_{Atc} and type IIB_{Atc} structures of (EH_2)-*-$\pi(C_{14}H_{10})$ were optimized for E = O and S, whereas only type IIB_{Atc} was optimized for E = Se and Te. The processes of the convergence are summarized in Table S1 of the ESI.‡

The type IIA_{Atc} structure optimized for (OH_2)-*-$\pi(C_{14}H_{10})$ with MP2/BSS-F was apparently different from type IIB_{Atc}, as confirmed by the r_1 values. In the case of $(SH_2)\cdots\pi(C_{14}H_{10})$, one structure was optimized, which was close to the type IIA_{Atc} structure if initially assuming a typical type IIA_{Atc} structure. The type IIA_{Atc} structure optimized for $(SH_2)\cdots\pi(C_{14}H_{10})$ [$SH_2\cdots\pi(C_{14}H_{10})$ (C_1: IIA_{Atc})] seems somewhat distorted from the C_s symmetry.[46] The search converged to another one, if started assuming typical type IIB_{Atc} and type IIC_{Atc} structures, which are close to type IIA_{Atc}. Indeed, their r_1 values are very close to each other, but the ϕ_2 and ϕ_3 values seem meaningfully different for the two types (Fig. 1c and d, respectively). Therefore, the second structure is (tentatively) called type IIB_{Atc}, herein. No type I_{Atc} structures were detected after similar treatment, even if optimizations started from those very close to type IA_{Atc}.

Table 1 collects the structural parameters selected for the optimized structures of (EH_2)-*-$\pi(C_{14}H_{10})$ (E = O, S, Se and Te), r_1, r_2, r_3, θ_1, θ_2, θ_3, ϕ_1, ϕ_2 and ϕ_3, which are defined in Scheme 2. The optimized structures are not shown in the figures, but they can be found in molecular graphs, which are drawn on the optimized structures (see Fig. 1). What factors appear to control the optimized structures? We compared the H···H distance in EH_2, r(H, H: EH_2), with the $^{11}C\cdots{}^{13}C$ distance in $C_{14}H_{10}$, $r(^{11}C, {}^{13}C$: $C_{14}H_{10})$. Indeed, r(H, H: EH_2) for E = O (1.522 Å), S (1.931 Å), Se (2.088 Å) and Te (2.361 Å) is shorter than $r(^{11}C, {}^{13}C$: $C_{14}H_{10})$ (2.452 Å for the central benzene ring), but the differences in r ($\Delta r = r$(C, C: $C_{14}H_{10}) - r$(H, H: EH_2)) are larger than 0.5 Å for O ($\Delta r = 0.9303$ Å) and S (0.5215 Å), whereas they are smaller than 0.4 Å for Se (0.3644 Å) and Te (0.0913 Å) (see Table S2 of the ESI‡). The type IIB_{Atc} structures of (EH_2)-*-$\pi(C_{14}H_{10})$ (E = O, S, Se and Te) would form with no limitations of Δr, whereas it may be necessary for Δr larger than around 0.5 Å to give the type IIA_{Atc} structures (E = O and S). In the case of type IIB_{Atc}, one H in EH_2 seems to be slightly above the $^{11}C\cdots{}^{13}C$ bond for E = S, Se and Te, but OH_2 seems to exist almost right above the $^{11}C\cdots{}^{13}C$ bond, which may also be controlled by Δr. Indeed, the difference in Δr between E = S and Se seems small, at a first glance, but the small difference would play an important role in the appearance of the type IIA_{Atc} structure.

What are the stabilization energies in the formation of the adducts? Table 1 contains the ΔE (ΔE_{ES} and ΔE_{Ent}) values for $(EH_2)\cdots\pi(C_{14}H_{10})$, where, ΔE_{ES} and ΔE_{Ent} are the ΔE values on the energy surfaces and those with the thermal corrections to enthalpies, respectively [$\Delta E = (E((EH_2)\cdots\pi(C_{14}H_{10})) - (E(EH_2) + E(C_{14}H_{10}))$]. An excellent correlation was obtained in the plot of ΔE_{Ent} *versus* ΔE_{ES} ($y = 5.262 + 1.047x$; $R_c^2 = 0.998$ ($n = 6$: number of data points)), although is not shown in the figure. Therefore,

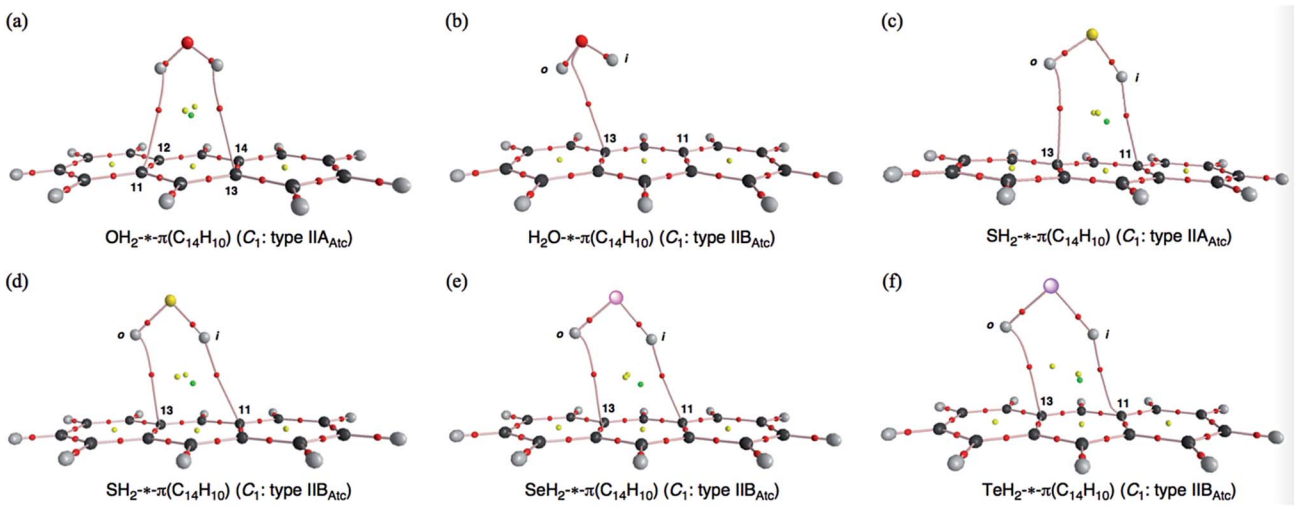

Fig. 1 Molecular graphs for OH_2-*-$\pi(C_{14}H_{10})$ (C_1: type IIA_{Atc}) (a), H_2O-*-$\pi(C_{14}H_{10})$ (C_1: type IIB_{Atc}) (b), SH_2-*-$\pi(C_{14}H_{10})$ (C_1: type IIA_{Atc}) (c), SH_2-*-$\pi(C_{14}H_{10})$ (C_1: type IIB_{Atc}) (d), SeH_2-*-$\pi(C_{14}H_{10})$ (C_1: type IIB_{Atc}) (e) and TeH_2-*-$\pi(C_{14}H_{10})$ (C_1: type IIB_{Atc}) (f), calculated with MP2/BSS-F. The bond critical points (BCPs) are denoted by red dots, ring critical points (RCPs) by yellow dots and cage critical points (CCPs) by green dots, together with bond paths by pink lines. Carbon atoms are in black and hydrogen atoms are in grey, with oxygen, sulphur, selenium and tellurium atoms in red, yellow, pink and purple, respectively.

Table 1 Structural parameters for $(EH_2)\cdots\pi(C_{14}H_{10})$ (E = O, S, Se and Te) optimized at the MP2 level with BSS-F[abc]

Species (X–Y) (symmetry: type)	r_1 (Å)	r_2 (Å)	r_3 (Å)	θ_1 (°)	θ_2 (°)	θ_3 (°)	ϕ_1 (°)	ϕ_2 (°)	ϕ_3 (°)	ΔE_{ES}[d] (kJ mol^{-1})	ΔE_{Ent}[e] (kJ mol^{-1})
$OH_2\cdots\pi(C_{14}H_{10})$ (C_1:[f] IIA_{Atc})	3.2865	0.9629	0.9629	89.9	51.8	103.5	−92.5	−1.7	2.8	−22.7	−18.1
$H_2O\cdots\pi(C_{14}H_{10})$ (C_1: IIB_{Atc})	3.6682	0.9631	0.9624	63.4	69.6	103.6	−93.8	−14.3	3.5	−21.9	−17.6
$SH_2\cdots\pi(C_{14}H_{10})$ (C_1: IIA_{Atc})[g]	3.6162	1.3389	1.3400	80.5	60.6	92.2	−92.1	−6.4	−3.3	−28.7	−25.0
$SH_2\cdots\pi(C_{14}H_{10})$ (C_1: IIB_{Atc})[g]	3.6165	1.3389	1.3400	80.5	60.6	92.2	−91.8	−2.1	−1.9	−28.7	−25.0
$SeH_2\cdots\pi(C_{14}H_{10})$ (C_1: IIB_{Atc})	3.6959	1.4597	1.4603	78.9	61.5	91.3	−91.5	3.0	−0.2	−31.7	−28.3
$TeH_2\cdots\pi(C_{14}H_{10})$ (C_1: IIB_{Atc})	3.7703	1.6576	1.6578	78.1	64.2	91.5	−89.9	−11.4	−17.5	−40.5	−36.8

[a] BSS-F: the 6-311+G(3df) basis set was employed for O, S and Se and the basis set of the (7433111/743111/7411/2 + 1s1p1d1f) type for Te with the 6-311++G(d,p) basis set for C and H. [b] See Scheme 2 for the structural parameters. [c] Optimized structures are not given in the figures but can be found in the molecular graphs drawn on the optimized structures (see Fig. 1). [d] $\Delta E_{ES} = E_{ES}((EH_2)\text{-}*\text{-}\pi(C_{14}H_{10})) - (E_{ES}(EH_2) + E_{ES}(C_{14}H_{10}))$ on the energy surface. [e] $\Delta E_{Ent} = E_{Ent}((EH_2)\text{-}*\text{-}\pi(C_{14}H_{10})) - (E_{Ent}(EH_2) + E_{Ent}(C_{14}H_{10}))$ with the thermal corrections to enthalpies. [f] Very close to C_s. [g] The structures are very close to each other; however, they are analysed as two different structures here since the differences in ϕ_2 and ϕ_3 seem meaningful. They are called IIA_{Atc} and IIB_{Atc}.

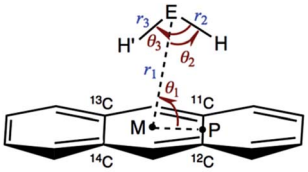

$\phi_1(^{11}CPME)$; ϕ_2(PMEH); ϕ_3(MEHH')

Type II_{Atc}

Scheme 2 Structural Parameters Illustrated for Type II_{Atc} of (EH_2)-*-$\pi(C_{14}H_{10})$ (E = O, S, Se and Te).

the ΔE_{ES} values will be employed for the discussion of ΔE. A good correlation was also obtained in the plot of ΔE_{ES} *versus* r_1, if the data for $H_2O\cdots\pi(C_{14}H_{10})$ (C_1: IIB_{Atc}) are neglected ($y = -1410.42 + 820.87x - 121.30x^2$; $R_c^2 = 0.975$ ($n = 5$)), where the structure of $H_2O\cdots\pi(C_{14}H_{10})$ (C_1: IIB_{Atc}) seems different from the others.

What are the relations between ΔE_{Atc}, ΔE_{Nap} and ΔE_{Bzn}? The ΔE_{Nap} values are linearly proportional to ΔE_{Bzn} in type II. The ratio of $\Delta E_{Nap}/\Delta E_{Bzn}$ becomes larger in the order of E = O ($\Delta E_{Nap}/\Delta E_{Bzn} = 1.34$) < S (1.60) < Se (1.68) < Te (1.75), which shows a substantial chalcogen dependence. On the other hand, the $\Delta E_{Atc}/\Delta E_{Nap}$ ratio seems almost constant for E = O ($\Delta E_{Atc}/\Delta E_{Nap} = 1.01$) < S (1.07) < Se (1.09) < Te (1.11). The different basis sets for Te may somewhat affect the evaluated values for E = Te, which are from the Sapporo Basis Set Factory, whereas the others are from the Gaussian09 program. What mechanisms operate to control the ratios? It is difficult to clarify this, however, we examined the ratios of $r_{1:Bzn}/r_{1:Nap}$ and $r_{1:Atc}/r_{1:Nap}$. The $r_{1:Bzn}/r_{1:Nap}$ ratios become larger in the order of 1.01 (E = O) < 1.13 (S) < 1.15 (Se) < 1.19 (Te) and the $r_{1:Atc}/r_{1:Nap}$ ratios increase similarly in the order of 1.00 (E = O) < 1.09 (S) < 1.11 (Se) < 1.13 (Te). However, the chalcogen dependence of the ratios seems somewhat smaller for $r_{1:Atc}/r_{1:Nap}$, relative to the case for $r_{1:Bzn}/r_{1:Nap}$. These results would be responsible for the observed $\Delta E/\Delta E$ ratios, although the vdW and/or covalent radii of chalcogens must also be carefully examined for the discussion.

Before the application of QTAIM-DFA to $(EH_2)\cdots\pi(C_{14}H_{10})$, the molecular graphs and contour plots are examined next.

Molecular graphs and contour plots of $\rho(r)$ for $(EH_2)\cdots\pi(C_{14}H_{10})$

Fig. 1 illustrates the molecular graphs for (EH_2)-*-$\pi(C_{14}H_{10})$ (E = O, S, Se and Te), which were calculated with MP2/BSS-F. The BCPs are clearly detected, which contain that expected between EH_2 and $C_{14}H_{10}$. Each BP with a BCP connects each H in EH_2 and the carbon atom of ^{11}C or ^{13}C in $C_{14}H_{10}$ for all optimized structures in Table 2, except for the type IIB_{Atc} of H_2O-*-$\pi(C_{14}H_{10})$. The BP with BCP joins O in OH_2 and a carbon atom of ^{11}C or ^{13}C in $C_{14}H_{10}$ of OH_2-*-$\pi(C_{14}H_{10})$. Therefore, the interactions between EH_2 and $C_{14}H_{10}$ are classified by π-HBs for all the adducts in Table 2, except for the type IIB_{Atc} of H_2O-*-$\pi(C_{14}H_{10})$, the interaction of which should be classified by the π-EB type. Ring critical points (RCPs) and cage critical points (CCPs) are also detected in Fig. 1. Fig. 2 shows the contour plots of $\rho(r)$ for $(EH_2)\cdots\pi(C_{14}H_{10})$ (E = O, S, Se and Te) calculated with MP2/BSS-F. The contour plots of $\rho(r)$ are drawn on a plane containing E, BCP (*) of the (EH_2)-*-π type and an atom or BCP suitable for the contour plots of (EH_2)-*-$\pi(C_{14}H_{10})$. The BCPs are well located at the (three dimensional) saddle points of $\rho(r)$ in the species. Negative Laplacians and trajectory plots are drawn in Fig. S2 and S3 of the ESI.‡ It is well visualized how the BCPs are classified through $\nabla^2\rho(r)$ and the space around the species is well divided by the atoms in it.

Survey of the interactions in (EH_2)-*-$\pi(C_{14}H_{10})$ (E = O, S, Se and Te)

As shown in Fig. 1 and 2, some BPs are apparently curved. Therefore, the lengths of the BPs (r_{BP}) will be substantially different from the straight-line distances (R_{SL}) in some cases. The r_{BP} and R_{SL} values are collected in Table S2 of the ESI‡ for (EH_2)-*-$\pi(C_{14}H_{10})$ (E = O, S, Se and Te), which were evaluated with MP2/BSS-F, together with the differences between r_{BP} and R_{SL} ($\Delta r_{BP} = r_{BP} - R_{SL}$). There are two types of BPs in each adduct since each adduct has C_1 symmetry. Therefore, it is necessary to define the BPs to distinguish the two. Letting ^{i}H and ^{o}H in EH_2 connect to $\pi(C_{14}H_{10})$ through BPs, which are placed more inside and more outside, respectively, in relation to the centre of $C_{14}H_{10}$, then ^{i}BP and ^{o}BP can be defined as ^{i}BP (^{i}**H**-*-π) and ^{o}BP (^{o}**H**-*-π), respectively.

Table 2 QTAIM functions and QTAIM-DFA parameters for the interactions in (EH_2)-*-π$(C_{14}H_{10})$ (E = O, S, Se and Te) evaluated with MP2/BSS-F[a]

Interaction (X-*-Y)[e]	Type[b]	$\rho_b(r_c)$ (ea_o^{-3})	$c\nabla^2\rho_b(r_c)$[c] (au)	$H_b(r_c)$ (au)	$k_b(r_c)$[d]	R (au)	θ (°)	Freq (cm^{-1})	k_f (unit[f])	θ_p (°)	κ_p (au^{-1})	Classification characterization
OHH-*-$^{11(13)}$C(π)	IIA_{Atc}[g]	0.0060	0.0024	0.0007	−0.814	0.0025	72.6	108.7	0.0411	74.5	8.0	p-CS/vdW
H_2O-*-^{13}C(π)	IIB_{Atc}	0.0069	0.0029	0.0009	−0.831	0.0031	73.9	104.5	0.0346	79.3	18.1	p-CS/vdW
S^oH^iH-*-^{11}C(π)[h]	IIA_{Atc}	0.0072	0.0027	0.0009	−0.807	0.0029	72.1	65.9	0.0151	72.2	1.1	p-CS/vdW
S^iH^oH-*-^{13}C(π)[h]	IIA_{Atc}	0.0065	0.0024	0.0007	−0.835	0.0025	74.2	65.9	0.0151	74.3	145.7	p-CS/vdW
S^oH^iH-*-^{11}C(π)[h]	IIB_{Atc}	0.0070	0.0027	0.0009	−0.799	0.0029	71.5	65.8	0.0161	73.6	37.3	p-CS/vdW
S^iH^oH-*-^{13}C(π)[h]	IIB_{Atc}	0.0065	0.0024	0.0007	−0.836	0.0025	74.2	65.8	0.0161	73.4	61.8	p-CS/vdW
Se^oH^iH-*-^{11}C(π)[h]	IIB_{Atc}	0.0072	0.0028	0.0010	−0.789	0.0029	70.8	54.6	0.0158	72.7	30.4	p-CS/vdW
Se^iH^oH-*-^{13}C(π)[h]	IIB_{Atc}	0.0070	0.0025	0.0007	−0.846	0.0026	75.0	54.6	0.0158	74.2	37.1	p-CS/vdW
Te^oH^iH-*-^{11}C(π)[h]	IIB_{Atc}	0.0077	0.0028	0.0008	−0.829	0.0029	73.7	50.5	0.0086	93.8	[i]	p-CS/*t*-HB_{nc}
Te^iH^oH-*-^{13}C(π)[h]	IIB_{Atc}	0.0088	0.0031	0.0008	−0.849	0.0032	75.3	23.9	0.0028	82.9	299.8	p-CS/vdW

[a] BSS-F: the 6-311+G(3df) basis set employed for O, S and Se and the basis set of the (7433111/743111/7411/2 + 1s1p1d1f) type for Te with the 6-311++G(d, p) basis set for C and H. [b] See Scheme 1 and Fig. 1. [c] $c\nabla^2\rho_b(r_c) = H_b(r_c) - V_b(r_c)/2$, where $c = \hbar^2/8m$. [d] $k_b(r_c) = V_b(r_c)/G_b(r_c)$. [e] The optimized structure has C_1 symmetry and atoms taking part in the interaction are shown in bold with BCP denoted by *. [f] mDyne $Å^{-1}$. [g] Very close to C_s symmetry. [h] ^{i}H and ^{o}H in EH_2 stand for the atoms taking part in the interactions, which are placed more inside and more outside, respectively, in relation to the centre of $C_{14}H_{10}$. [i] Vary large value of 1259 au^{-1}.

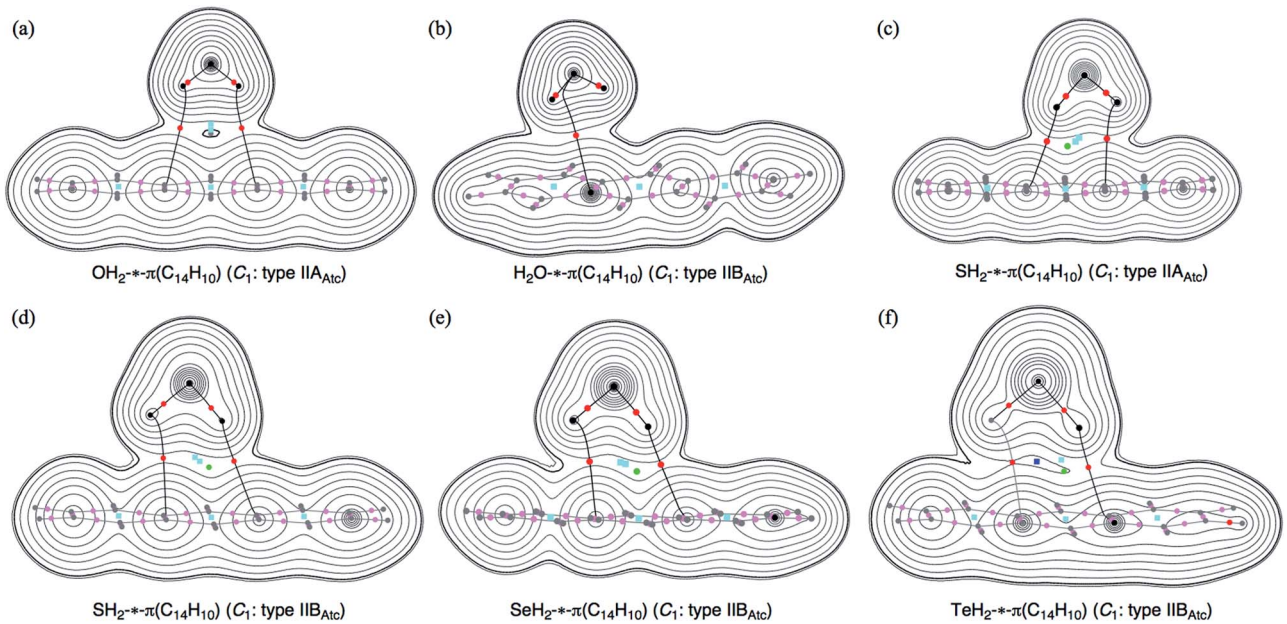

Fig. 2 Contour plots of $\rho(r)$ for OH_2-*-$(C_{14}H_{10})$ (C_1: type IIA_{Atc}) (a), H_2O-*-$(C_{14}H_{10})$ (C_1: type IIB_{Atc}) (b), SH_2-*-$(C_{14}H_{10})$ (C_1: type IIA_{Atc}) (c), SH_2-*-$(C_{14}H_{10})$ (C_1: type IIB_{Atc}) (d), SeH_2-*-$(C_{14}H_{10})$ (C_1: type IIB_{Atc}) (e) and TeH_2-*-$(C_{14}H_{10})$ (C_1: type IIB_{Atc}) (f), calculated with MP2/BSS-F. The BCPs on the plane are denoted by red dots, those outside of the plane in dark pink dots, RCPs by blue squares, CCPs by green dots and bond paths on the plane by black line and those outside of the plane are by grey lines. Carbon atoms are in black and hydrogen atoms are in grey, with the other atoms in black. The contours (ea_0^{-3}) are at 2^l ($l = \pm 8, \pm 7, \ldots, 0$) with 0.0047 (heavy line).

The Δr_{BP} values are small (*ca.* 0.03 Å) for ^{i}BP (S^oH^iH-*-^{11}C(π)) and ^{i}BP (Se^oH^iH-*-^{11}C(π)) in (EH_2-*-π$(C_{14}H_{10})$) (C_1: IIB_{Atc}). Thus, the ^{i}BPs can be approximated as straight lines. However, the Δr_{BP} value is large (0.41 Å) for ^{o}BP (Se^iH^oH-*-^{11}C(π)), which seems difficult to be approximated by a straight line. The values seem moderate (0.09–0.17 Å) for most of the π-HB and π-EB interactions in EH_2-*-π$(C_{14}H_{10})$ for E = O, S, Se and Te, other than three cases. The BPs could be approximated as almost straight lines to gentle curves. The r_{BP} values are plotted *versus* R_{SL} in Fig. 3. A very good correlation was obtained for the case of $0.09 \leq \Delta r_{BP} \leq 0.17$ Å, which is shown in the figure. The data for three BPs deviate from the correlation, although two of them can be approximated as straight lines, as mentioned above.

QTAIM-DFA was applied to the interactions between EH_2 and $C_{14}H_{10}$ in EH_2-*-π$(C_{14}H_{10})$ (E = O, S, Se and Te) and the QTAIM functions were calculated for the interactions at BCP. The results are given in Table 2. Fig. 4 shows the plot of $H_b(r_c)$ *versus* $H_b(r_c) - V_b(r_c)/2$ for EH_2-*-π$(C_{14}H_{10})$ (E = O, S, Se and Te), which contains the data for the perturbed structures evaluated with MP2/BSS-F. All the data in Fig. 4 appear in the area of $H_b(r_c) - V_b(r_c)/2 > 0$ and $H_b(r_c) > 0$, which belongs to the pure-CS (closed shell: p-CS) region. The plots were analysed according

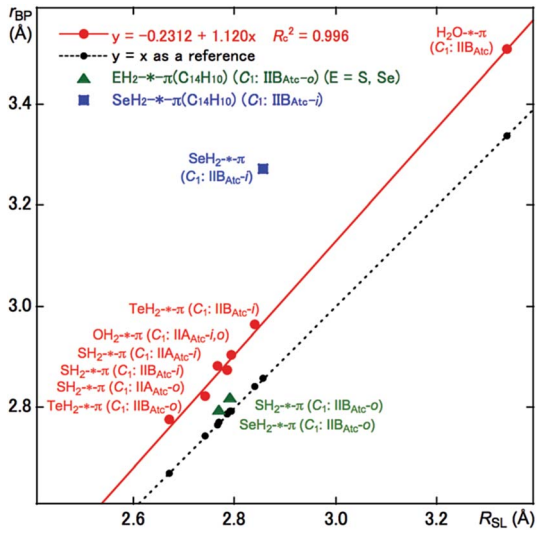

Fig. 3 Plots of r_{BP} *versus* R_{SL} for (EH_2)-*-π$(C_{14}H_{10})$ (E = O, S, Se and Te), evaluated with BSS-F at the MP2 level.

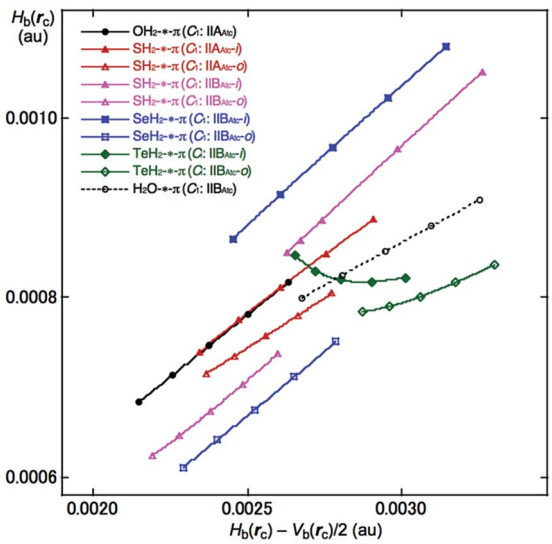

Fig. 4 Plots of $H_b(r_c)$ *versus* $H_b(r_c) - V_b(r_c)/2$ for (EH_2)-*-π$(C_{14}H_{10})$, evaluated with MP2/BSS-F. Compounds with marks are shown in the figure.

to eqn (S3)–(S6) of the ESI‡ by applying QTAIM-DFA. These results are discussed next.

Nature of π-HBs and π-EBs in EH_2-*-π$(C_{14}H_{10})$ (E = O, S, Se and Te)

Table 2 collects the QTAIM-DFA parameters of (R, θ) and (θ_p, κ_p) for the π-HB and π-EB interactions, together with the frequencies and the force constants (k_f) correlated to NIV, which are employed to generate the perturbed structures. The nature of π-HBs and π-EBs in EH_2-*-π$(C_{14}H_{10})$ is discussed based on the (R, θ, θ_p) values employing the standard values as a reference (see Scheme S2 of the ESI‡). It should be instructive to survey the criteria related to that herein before a detailed discussion. The criteria tell us that $45° < \theta < 90°$ for pure-CS interactions. The θ_p value predicts the character of the interactions. In the p-CS region, the character of the interactions will be the vdW type for $45° < \theta_p < 90°$, whereas it will be the *t*-HB (typical hydrogen bonds) type with no covalency (*t*-HB_{nc}) for $90° < \theta_p \leq 125°$, where $\theta_p = 125°$ tentatively corresponds to $\theta = 90°$.

The θ and θ_p values are less than 90° for all the π-HBs and π-EB in EH_2-*-π$(C_{14}H_{10})$ examined herein, except for the Te^iH^oH-*-$^{11}C(\pi)$ interaction in TeH_2-*-π$(C_{14}H_{10})$. Therefore, the π-HBs and π-EB interactions in EH_2-*-π$(C_{14}H_{10})$ in Table 2 are all classified by the pure-CS interactions and characterized as the vdW type (p-CS/vdW), except for Te^iH^oH-*-$^{11}C(\pi)$ in TeH_2-*-π$(C_{14}H_{10})$. Although ^{o}BP (Te^iH^oH-*-$^{13}C(\pi)$) is predicted to have the nature of (p-CS/vdW), ^{i}BP (Te^iH^oH-*-$^{11}C(\pi)$) is predicted to have the nature of (p-CS/*t*-HB_{nc}). The π-EB interaction in the H_2O-*-$^{11}C(\pi)$ type $[(\theta, \theta_p) = (73.9°, 79.3°)]$ is predicted to be somewhat stronger than the π–HB interaction of the OHH-*-$^{11}C(\pi)$ type $[(\theta, \theta_p) = (72.6°, 74.5°)]$ for OH_2-*-π$(C_{14}H_{10})$. The π-HB interactions in the anthracene system are predicted to be very similar to that in the naphthalene system, which seem slightly stronger than that in the benzene system. The results are in accordance with that derived from the energies for the formation of the adducts.

The delocalization indexes and ellipticity are the important parameters to clarify and understand the nature of the $(EH_2)\cdots\pi$ interactions.[47] The nature of the $(EH_2)\cdots\pi$ interactions will be discussed elsewhere based on these parameters for the series of $(EH_2)\cdots\pi(C_6H_6)$, $(EH_2)\cdots\pi(C_{10}H_8)$, and $(EH_2)\cdots\pi(C_{14}H_{10})$ (E = O, S, Se and Te).

Conclusions

The behaviour of the interactions for EH_2 adducts with the anthracene π-system (E = O, S, Se and Te) in a 1 : 1 ratio is elucidated by applying QTAIM-DFA. The structures were optimized with MP2/BSS-F. Two types of structures were optimized for E = O and S, whereas one was optimized for E = Se and Te. The BCPs are clearly detected in the molecular graphs. The interactions are the π-HB type for EH_2-*-π$(C_{14}H_{10})$ (C_1: IIA_{Atc}) (E = O and S) and EH_2-*-π$(C_{14}H_{10})$ (C_1: IIB_{Atc}) (E = S, Se and Te), whereas they are the π-EB type for H_2O-*-π$(C_{14}H_{10})$ (C_1: IIB_{Atc}). The QTAIM-DFA parameters of (R, θ) and (θ_p, κ_p) are calculated for the species, according to eqn (S3)–(S6).‡ The θ values are less than 90° for all interactions examined in this work. The θ_p values are also less than 90° for all the interactions in question, except for ^{i}H-*-$^{11}C(\pi)$ in TeH_2-*-$C_{14}H_{10}$ (C_1: IIB_{Atc}). Therefore, all the π-HB and π-EB interactions examined in this work are classified by pure-CS interactions and characterized as vdW in nature (p-CS/vdW), although ^{i}H-*-$^{11}C(\pi)$ in TeH_2-*-$C_{14}H_{10}$ (C_1: IIB_{Atc}) is predicted to have the p-CS/*t*-HB nature without covalency. The π-EB interaction is predicted to be somewhat stronger than π-HB in (OH_2)-*-π$(C_{14}H_{10})$. It is demonstrated that the predicted nature of EH_2-*-π$(C_{14}H_{10})$ is closer to that of EH_2-*-π$(C_{10}H_8)$ rather than that of EH_2-*-π(C_6H_6). The π-HB and π-EB interactions in the anthracene π-system are well elucidated by applying QTAIM-DFA.

Acknowledgements

This work was partially supported by a Grant-in-Aid for Scientific Research (No. 26410050) from the Ministry of Education, Culture, Sports, Science and Technology, Japan. The support of the Wakayama University Original Research Support Project Grant and the Wakayama University Graduate School Project Research Grant is also acknowledged.

Notes and references

1 Y. Sugibayashi, S. Hayashi and W. Nakanishi, *ChemPhysChem*, 2016, **17**, 2579–2589.
2 S. Hayashi, Y. Sugibayashi and W. Nakanishi, *Phys. Chem. Chem. Phys.*, 2016, **18**, 9948–9960.
3 S. Suzuki, P. G. Green, R. E. Bumgarner, S. Dasgupta, W. A. Goddard III and G. A. Blake, *Science*, 1992, **257**, 942–945. See also; R. N. Pribble and T. S. Zwier, *Science*, 1994, **265**, 75–79; X. Wang and P. P. Power, *Angew. Chem., Int. Ed.*, 2011, **50**, 10965–10968.
4 K. P. Gierszal, J. G. Davis, M. D. Hands, D. S. Wilcox, L. V. Slipchenko and D. Ben-Amotz, *J. Phys. Chem. Lett.*, 2011, **2**, 2930–2933.
5 J. Ma, D. Alfe, A. Michaelides and E. Wang, *J. Chem. Phys.*, 2009, **130**, 154303–154304.
6 S. Li, V. R. Cooper, T. Thonhauser, A. Puzder and D. C. Langreth, *J. Phys. Chem. A*, 2008, **112**, 9031–9036.
7 T. P. Tauer, M. E. Derrick and C. D. Sherrill, *J. Phys. Chem. A*, 2005, **109**, 191–196.
8 T. Takatani and C. D. Sherrill, *Phys. Chem. Chem. Phys.*, 2007, **9**, 6106–6114.
9 E. M. Cabaleiro-Lago, J. Rodriguez-Otero and A. Pena-Gallego, *J. Phys. Chem. A*, 2008, **112**, 6344–6350.
10 H. S. Biswal and S. Wategaonkar, *J. Phys. Chem. A*, 2009, **113**, 12774–12782.
11 S. Hayashi, Y. Sugibayashi and W. Nakanishi, *RSC Adv.*, 2016, **6**, 49651–49660.
12 L. Pauling, *The Nature of the Chemical Bond*, ed. L. Pauling, Cornell University Press, Ithaca, NY, 3rd edn, 1960.
13 S. Kozmon, R. Matuška, V. Spiwok and J. Koča, *Phys. Chem. Chem. Phys.*, 2011, **13**, 14215–14222.
14 J. M. Hermida-Ramon and A. M. Grana, *J. Comput. Chem.*, 2007, **28**, 540–546.
15 C. D. Zeinalipour-Yazdi and D. P. Pullman, *J. Phys. Chem. B*, 2006, **110**, 24260–24265.
16 T. Sato, T. Tsuneda and K. Hirao, *J. Chem. Phys.*, 2005, **123**, 104307.
17 S. Tsuzuki, K. Honda, T. Uchimaru and M. Mikami, *J. Chem. Phys.*, 2004, **120**, 647–659.
18 A. Reyes, M. A. Tlenkopatchev, L. Fomina, P. Guadarrama and S. Fomine, *J. Phys. Chem. A*, 2003, **107**, 7027–7031.
19 T. R. Walsh, *Chem. Phys. Lett.*, 2002, **363**, 45–51.
20 B. Collignon, P. N. M. Hoang, S. Picaud, D. Liotard, M. T. Rayez and J. C. Rayez, *J. Mol. Struct.: THEOCHEM*, 2006, **772**, 1–12.
21 A chemical bond or an interaction between A and B is denoted by A–B, which corresponds to BPs between A and B in QTAIM. A-*-B is employed here to emphasize the presence of BCP on A–B, although A-•-B would be more suitable since dots are usually used to represent BCPs on BPs.
22 *Atoms in Molecules. A Quantum Theory*, ed. R. F. W. Bader, Oxford University Press, Oxford, UK, 1990.
23 C. F. Matta and R. J. Boyd, *An Introduction to the Quantum Theory of Atoms in Molecules In The Quantum Theory of Atoms in Molecules: From Solid State to DNA and Drug Design*, ed. C. F. Matta and R. J. Boyd, Wiley-VCH, Weinheim, Germany, 2007, ch. 1.
24 (*a*) R. F. W. Bader, T. S. Slee, D. Cremer and E. Kraka, *J. Am. Chem. Soc.*, 1983, **105**, 5061–5068; (*b*) R. F. W. Bader, *Chem. Rev.*, 1991, **91**, 893–928; (*c*) R. F. W. Bader, *J. Phys. Chem. A*, 1998, **102**, 7314–7323; (*d*) F. W. Biegler-König, R. F. W. Bader and T. H. Tang, *J. Comput. Chem.*, 1982, **3**, 317–328; (*e*) R. F. W. Bader, *Acc. Chem. Res.*, 1985, **18**, 9–15; (*f*) T. H. Tang, R. F. W. Bader and P. MacDougall, *Inorg. Chem.*, 1985, **24**, 2047–2053; (*g*) F. Biegler-König, J. Schönbohm and D. Bayles, *J. Comput. Chem.*, 2001, **22**, 545–559; (*h*) F. Biegler-König and J. Schönbohm, *J. Comput. Chem.*, 2002, **23**, 1489–1494.
25 J. A. Dobado, H. Martînez-Garcîa, J. Molina and M. R. Sundberg, *J. Am. Chem. Soc.*, 2000, **122**, 1144–1149.
26 J. Molina and J. A. Dobado, *Theor. Chem. Acc.*, 2001, **105**, 328–337.
27 S. K. Ignatov, N. H. Rees, B. R. Tyrrell, S. R. Dubberley, A. G. Razuvaev, P. Mountford and G. I. Nikonov, *Chem.–Eur. J.*, 2004, **10**, 4991–4999.
28 S. K. Tripathi, U. Patel, D. Roy, R. B. Sunoj, H. B. Singh, G. Wolmershäuser and R. J. Butcher, *J. Org. Chem.*, 2005, **70**, 9237–9247.
29 (*a*) M. Yamashita, Y. Yamamoto, K.-Y. Akiba, D. Hashizume, F. Iwasaki, N. Takagi and S. Nagase, *J. Am. Chem. Soc.*, 2005, **127**, 4354–4371; (*b*) Y. Yamamoto and K.-Y. Akiba, *J. Synth. Org. Chem., Jpn.*, 2004, **62**, 1128–1137.
30 W. Nakanishi, T. Nakamoto, S. Hayashi, T. Sasamori and N. Tokitoh, *Chem.–Eur. J.*, 2007, **13**, 255–268.
31 Interactions would be easily imaged by means of QTAIM if they can be defined as the corresponding bond paths (BPs), especially for experimental chemists. However, it is demonstrated that the detection of the BPs between two atoms in a molecule emerging from natural alignment of the gradient vector field of the one-electron density of a molecule is neither necessary nor a sufficient condition for the presence of a chemical bond between those atoms.[48] In this connection, it is pointed out that the terms line paths (LPs) and line critical points (LCPs) should be used in place of BPs and BCPs, respectively.[48b] Consequently, the dynamic and static nature in this work should be regarded as the investigation performed at LCPs on LPs corresponding to the EH_2-π interactions in the anthracene-π system. Nevertheless, BPs and BCPs are used in this paper for the discussion of the EH_2-π($C_{14}H_{10}$) interactions, similarly to the case of the previous discussion for the EH_2-π(C_6H_6) and EH_2-π($C_{10}H_8$) interactions. The interactions expected between EH_2 and

$\pi(C_{14}H_{10})$ are clearly detected by BPs with BCPs which is another reason to use BPs and BCPs in this work.

32 Critical points (CPs) are characterized by the rank (ω) and the signature (σ). The CPs of the species in the three-dimensional space are classified by $\omega = 3$, which generally corresponds to all species. On the other hand, σ is defined by the simple algebraic sum of the signs of $\partial^2\rho_b(r_c)/\partial r_i^2$ ($r_i = x$, y and z for $i = 1$, 2 and 3, respectively), where the + and − signs of $\partial^2\rho_b(r_c)/\partial r_i^2$ are counted as +1 and −1, respectively. Therefore, $\sigma = -3$, −1, 1 and 3 correspond to attractors (nuclei), bond critical points (BCPs), ring critical points (RCPs) and cage critical points (CCPs), respectively. Namely, BCP is characterized by $(\omega, \sigma) = (3, -1)$.[17,18]

33 (*a*) W. Nakanishi, S. Hayashi and K. Narahara, *J. Phys. Chem. A*, 2009, **113**, 10050–10057; (*b*) W. Nakanishi, S. Hayashi and K. Narahara, *J. Phys. Chem. A*, 2008, **112**, 13593–13599.

34 W. Nakanishi and S. Hayashi, *Curr. Org. Chem.*, 2010, **14**, 181–197.

35 W. Nakanishi and S. Hayashi, *J. Phys. Chem. A*, 2010, **114**, 7423–7430.

36 W. Nakanishi, S. Hayashi, K. Matsuiwa and M. Kitamoto, *Bull. Chem. Soc. Jpn.*, 2012, **85**, 1293–1305.

37 See also, D. Cremer and E. Kraka, *Angew. Chem., Int. Ed.*, 1984, **23**, 627–628.

38 QTAIM-DFA is successfully applied to analyse weak to strong interactions in the gas phase. It could also be applied to the interactions in crystals and that in larger systems containing bioactive materials. The methodological improvement is inevitable to generate perturbed structures suitable for the systems.

39 The concept of a dynamic molecular graph was recently proposed by Corte's-Guzma'n and co-workers through the investigation of the Born–Oppenheimer molecular dynamics (BOMD), which was exemplified by [Fe{C-$(CH_2)_3$}$(CO)_3$]. The investigation illustrates the change in the behaviour of the molecular graph.[49] The concept of the dynamic molecular graph would be closely related to that of the dynamic nature of interactions predicted by employing the perturbed structures generated with the normal coordinate of internal vibrations (NIV). In this treatment, the selected vibration for NIV must contain the motion of the interaction in question most effectively among all the zero-point internal vibrations. A structural catastrophe is confirmed not to occur for the perturbed and fully optimized structures for the elucidation of the dynamic nature of the interaction in question with NIV.[35].

40 M. J. Frisch, G. W. Trucks, H. B. Schlegel, G. E. Scuseria, M. A. Robb, J. R. Cheeseman, G. Scalmani, V. Barone, B. Mennucci, G. A. Petersson, H. Nakatsuji, M. Caricato, X. Li, H. P. Hratchian, A. F. Izmaylov, J. Bloino, G. Zheng, J. L. Sonnenberg, M. Hada, M. Ehara, K. Toyota, R. Fukuda, J. Hasegawa, M. Ishida, T. Nakajima, Y. Honda, O. Kitao, H. Nakai, T. Vreven, J. A. Montgomery Jr, J. E. Peralta, F. Ogliaro, M. Bearpark, J. J. Heyd, E. Brothers, K. N. Kudin, V. N. Staroverov, R. Kobayashi, J. Normand, K. Raghavachari, A. Rendell, J. C. Burant, S. S. Iyengar, J. Tomasi, M. Cossi, N. Rega, J. M. Millam, M. Klene, J. E. Knox, J. B. Cross, V. Bakken, C. Adamo, J. Jaramillo, R. Gomperts, R. E. Stratmann, O. Yazyev, A. J. Austin, R. Cammi, C. Pomelli, J. W. Ochterski, R. L. Martin, K. Morokuma, V. G. Zakrzewski, G. A. Voth, P. Salvador, J. J. Dannenberg, S. Dapprich, A. D. Daniels, Ö. Farkas, J. B. Foresman, J. V. Ortiz, J. Cioslowski and D. J. Fox, *Gaussian 09 (Revision D.01)*, Gaussian, Inc., Wallingford CT, 2009.

41 For the 6-311G basis sets, see: (*a*) R. C. Binning Jr and L. A. Curtiss, *J. Comput. Chem.*, 1990, **11**, 1206–1216; (*b*) L. A. Curtiss, M. P. McGrath, J.-P. Blaudeau, N. E. Davis, R. C. Binning Jr and L. Radom, *J. Chem. Phys.*, 1995, **103**, 6104–6113; (*c*) M. P. McGrath and L. Radom, *J. Chem. Phys.*, 1991, **94**, 511–516. For the diffuse functions (+ and ++), see: T. Clark, J. Chandrasekhar, G. W. Spitznagel and P. V. R. Schleyer, *J. Comput. Chem.*, 1983, **4**, 294–301.

42 T. Noro, M. Sekiya and T. Koga, *Theor. Chem. Acc.*, 2012, **131**, 1124.

43 (*a*) C. Møller and M. S. Plesset, *Phys. Rev.*, 1934, **46**, 618–622; (*b*) J. Gauss, *J. Chem. Phys.*, 1993, **99**, 3629–3643; (*c*) J. Gauss, *Ber. Bunsen-Ges. Phys. Chem.*, 1995, **99**, 1001–1008.

44 The AIM2000 program (Version 2.04) is employed to analyze and visualize atoms-in-molecules: F. Biegler-König, *J. Comput. Chem.*, 2000, **21**, 1040–1048. See also ref. 24*g*.

45 S. Hayashi, K. Matsuiwa, M. Kitamoto and W. Nakanishi, *J. Phys. Chem. A*, 2013, **117**, 1804–1816.

46 The C_s structure of SH_2–$\pi(C_{14}H_{10})$ (IIA_{Atc}) was also obtained if optimized with MP2/BSS-F′, where 6-311+G(d,p) was employed for C and H in place of 6-311++G(d,p) in BSS-F′. However, the optimized structures with MP2/BSS-F′, which all had positive frequencies, were also C_1, although they seem slightly closer to C_s.

47 G. V. Baryshnikov, B. F. Minaev, V. A. Minaeva, A. T. Baryshnikova and M. Pittelkow, *J. Mol. Struct.*, 2012, **1026**, 127–132; G. V. Baryshnikov, B. F. Minaev, V. A. Minaeva and V. G. Nenajdenko, *J. Mol. Model.*, 2013, **19**, 4511–4519; N. N. Karaush, G. V. Baryshnikov, V. A. Minaeva and B. F. Minaev, *New J. Chem.*, 2015, **39**, 7815–7821; N. N. Karaush, G. V. Baryshnikov and B. F. Minaev, *RSC Adv.*, 2015, **5**, 24299–24305.

48 (*a*) R. F. W. Bader, *J. Phys. Chem. A*, 2009, **113**, 10391–10396; (*b*) C. Foroutan-Nejad, S. Shahbazian and R. Marek, *Chem.–Eur. J.*, 2012, **18**, 4982–4993; (*c*) M. García-Revilla, E. Francisco, P. L. A. Popelier and A. M. Pendás, *ChemPhysChem*, 2013, **14**, 1211–1218; (*d*) Z. A. Keyvani, S. Shahbazian and M. Zahedi, *Chem.–Eur. J.*, 2016, **22**, 5003–5009.

49 F. Cortés-Guzmán, T. Rocha-Rinza, J. M. Guevara-Vela, G. Cuevas and R. M. Gómez, *Chem.–Eur. J.*, 2014, **20**, 5665–5672.